AD-A137 752 MICROWAVE EMISSION FROM RELATIVISTIC ELECTRON BEAMS(U) 1/1
MASSACHUSETTS INST OF TECH CAMBRIDGE RESEARCH LAB OF
ELECTRONICS G BEKEFI 23 DEC 83 AFOSR-TR-84-0027
UNCLASSIFIED F49620-83-C-0008 F/G 20/8 NL

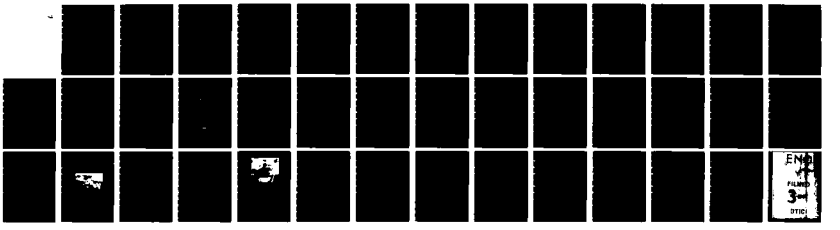

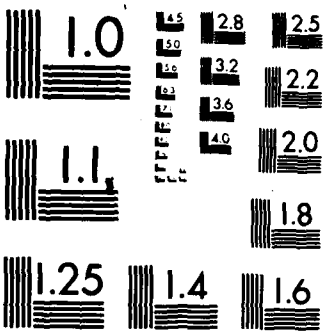

MICROCOPY RESOLUTION TEST CHART
NATIONAL BUREAU OF STANDARDS-1963-A

(12)

Final Report

Microwave Emission from Relativistic Electron Beams

Air Force Office of Scientific Research

Contract F49620-83-C-0008

covering the period

1 October 1982 - 31 October 1983

Submitted by

George Bekefi

December 23, 1983

MASSACHUSETTS INSTITUTE OF TECHNOLOGY
Research Laboratory of Electronics
Cambridge, Massachusetts 02139

UNCLASSIFIED

SECURITY CLASSIFICATION OF THIS PAGE

REPORT DOCUMENTATION PAGE

1a. REPORT SECURITY CLASSIFICATION Unclassified	1b. RESTRICTIVE MARKINGS
2a. SECURITY CLASSIFICATION AUTHORITY	3. DISTRIBUTION/AVAILABILITY OF REPORT Approved for public release; distribution unlimited
2b. DECLASSIFICATION/DOWNGRADING SCHEDULE	
4. PERFORMING ORGANIZATION REPORT NUMBER(S)	5. MONITORING ORGANIZATION REPORT NUMBER(S) AFOSR-TR- 84-0027
6a. NAME OF PERFORMING ORGANIZATION Massachusetts Institute of Technology 6b. OFFICE SYMBOL (If applicable)	7a. NAME OF MONITORING ORGANIZATION AFOSR
6c. ADDRESS (City, State and ZIP Code) Cambridge, MA 02139	7b. ADDRESS (City, State and ZIP Code) Bolling AFB Washington, DC 20332
8a. NAME OF FUNDING/SPONSORING ORGANIZATION AFOSR 8b. OFFICE SYMBOL (If applicable) NP	9. PROCUREMENT INSTRUMENT IDENTIFICATION NUMBER F49620-83-C-0008
8c. ADDRESS (City, State and ZIP Code) Bolling AFB, Wash DC, 20332	10. SOURCE OF FUNDING NOS. PROGRAM ELEMENT NO. 61102F; PROJECT NO. 2301; TASK NO. A1; WORK UNIT NO.
11. TITLE (Include Security Classification) MICROWAVE EMISSION FROM RELATIVISTIC ELECTRON BEAMS	
12. PERSONAL AUTHOR(S) George Bekefi	
13a. TYPE OF REPORT FINAL 13b. TIME COVERED FROM 1 Oct 82 TO 31 Oct 83	14. DATE OF REPORT (Yr., Mo., Day) 23 Dec 83 15. PAGE COUNT 38
16. SUPPLEMENTARY NOTATION	
17. COSATI CODES FIELD / GROUP / SUB. GR.	18. SUBJECT TERMS (Continue on reverse if necessary and identify by block number)

19. ABSTRACT (Continue on reverse if necessary and identify by block number)

During the past year we have carried out microwave and millimeter wave emission experiments on three systems that are described below. System one is a Rippled-Field Magnetron and represents a hybrid between a conventional magnetron and a free electron laser. System two is a Circular Free Electron Laser in which a rotating ring of relativistic electrons is subjected to an azimuthally periodic magnetic field. This work was carried out in cooperation with Professor W.W. Destler at the University of Maryland. Professor Destler has an accelerator capable of producing relativistic electron rings, and it is on this facility that our experiments were carried out. The third system concerns an inverted Relativistic Magnetron. The latter work is now finished and the results have appeared in the Journal of Applied Physics, 54, 4147 (1983).

20. DISTRIBUTION/AVAILABILITY OF ABSTRACT UNCLASSIFIED/UNLIMITED ☒ SAME AS RPT. ☒ DTIC USERS ☐	21. ABSTRACT SECURITY CLASSIFICATION Unclassified
22a. NAME OF RESPONSIBLE INDIVIDUAL	22b. TELEPHONE NUMBER (Include Area Code) 22c. OFFICE SYMBOL

DD FORM 1473, 83 APR EDITION OF 1 JAN 73 IS OBSOLETE.

UNCLASSIFIED

SECURITY CLASSIFICATION OF THIS PAGE

SUMMARY OF RESEARCH CARRIED OUT BETWEEN OCTOBER 1, 1982 - OCTOBER 31, 1983

During the past year we have carried out microwave and millimeter wave emission experiments on three systems that are described below.

System one is a Rippled-Field Magnetron and represents a hybrid between a conventional magnetron and a free electron laser. System two is a Circular Free Electron Laser in which a rotating ring of relativistic electrons is subjected to an azimuthally periodic magnetic field. This work was carried out in cooperation with Professor W.W. Destler at the University of Maryland. Professor Destler has an accelerator capable of producing relativistic electron rings, and it is on this facility that our experiments were carried out. The third system concerns an inverted Relativistic Magnetron. The latter work is now finished and the results have appeared in the Journal of Applied Physics, 54, 4147 (1983).

1. RIPPLED FIELD MAGNETRONS

To achieve efficient conversion of energy from a stream of free electrons to electromagnetic radiation, near synchronism must be attained between the velocity of the electrons and the phase velocity of the wave. In crossed-field devices, of which the magnetron is a typical example, this synchronism occurs between electrons undergoing a $v=\vec{E}_0\times\vec{B}_0$ drift in orthogonal electric and magnetic fields, and an electromagnetic wave whose velocity is reduced by a slow-wave structure comprised of a periodic assembly of resonant cavities. The complex system of closely spaced resonators embedded in the anode block limits the conventional magnetron to wavelengths in the centimeter range. Moreover, at high voltages typical of relativistic magnetrons, RF or dc breakdown in the electron beam interaction space, and at the sharp resonator edges poses serious problems.

The rippled-field magnetron is a novel source of coherent radiation devoid of physical slow-wave structures and capable of radiating at much higher frequen-

cies than a conventional magnetron. The configuration of the anode and cathode is similar to the so-called "smooth-bore" magnetron, but it differs from the latter in that the electrons are subjected to an additional field, an azimuthally periodic (wiggler) magnetic field B_w oriented transversely to the flow velocity v. The resulting $-e\vec{v}\times\vec{B}_w$ force gives the electrons an undulatory motion which effectively increases their velocity, and allows them to become synchronous with one of the fast TE or TM electomagnetic modes (phase velocity > c) characteristic of the smooth-bore magnetron. We note that this technique is also the basis of free-electron lasers (FEL). This device differs from the FEL in that the electron source (the cathode) and the acceleration region (the anode-cathode gap) are integral parts of the RF interaction space. This makes for high space-charge densities and for large growth rate of the FEL instability. The magnetron configuration is cylindrical rather than linear as in conventional FEL's, and the system is therefore very compact. The cylindrical geometry also allows for a continuous circulation of the growing electromagnetic wave, and because of this internal feedback, the rippled-field magnetron is basically an oscillator rather than an amplifier as is the case of the FEL.

We have obtained measurements of millimeter wave emission from the rippled field magnetron. This device is a hybrid between a smooth-bore magnetron and a free electron laser in which electrons move under the combined action of a radial electric field, a uniform axial magnetic field and an azimuthally periodic wiggler magnetic field.

A schematic of the magnetron cavity is shown in Fig. 1. It comprises a smooth cylindrical field emission cathode of radius 5.22cm enclosing a smooth cylindrical anode 4.43cm in radius. A Physics International Pulserad 110A

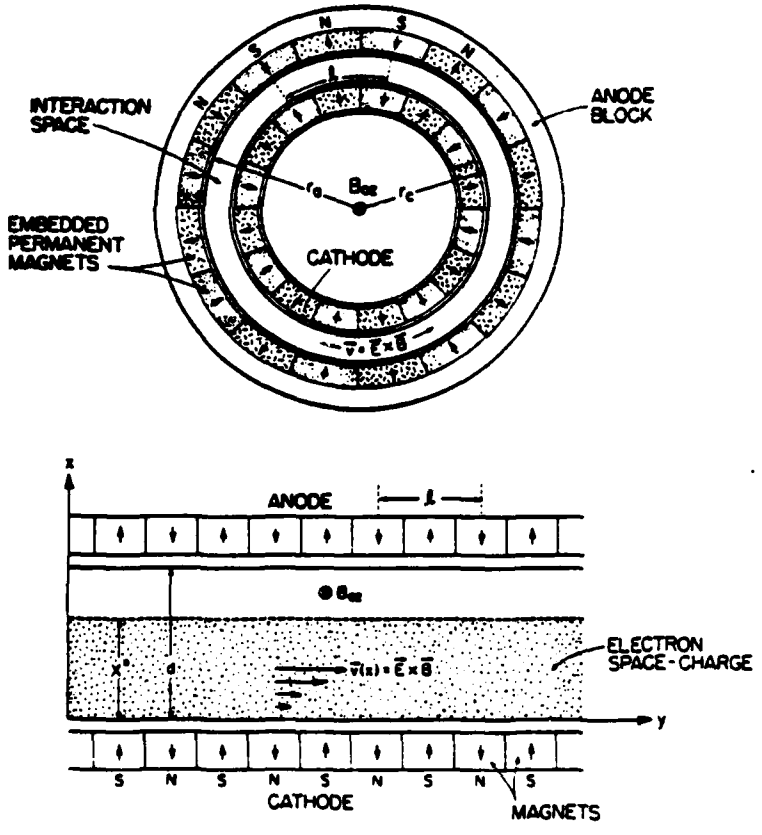

Fig. 1. Schematic diagram of a rippled-field magnetron (top) and a planar version of the device (bottom).

(V=0.7-1.4MV) accelerator supplies a radial electric field across the anode-cathode gap for approximately 30ns. The coaxial cavity is surrounded by two pulsed magnetic field coils which provide a uniform axial magnetic field of 6-15kG in the interaction space. The wiggler magnetic field is produced by a periodic assembly of samarium-cobalt bar magnets positioned behind the smooth stainless steel electrodes. The wiggler field midway between the electrodes is primarily radial and has a periodicity L=5.06, 2.53, or 1.26cm depending on the orientation of the magnets. For these periodicities, radial wiggler field amplitudes B_w=2.26, 1.96, and 0.68kG respectively are obtained.

Millimeter wave power and frequency measurements were performed in three frequency bands 2-4GHz, 7-12GHz, and 26.5-60GHz. Frequency spectra were obtained with solid state and waveguide dispersive lines and with a millimeter wave grating spectrometer. Absolute power levels were measured with calibrated crystal detectors.

Maximum radiated power in the 26.5-60GHz frequency band is obtained with L=2.53cm and B_w=1.96kG. Under these conditions a narrow band spectral line is observed with a line width at the half power points less than 2.2GHz. The center frequency of this line can be varied from 32GHz to 46GHz by varying B_z between 5.8kG and 9kG. No deterioration in line profile is observed over this range. The total radiated power above 26.5GHz measured with this wiggler is 300kW; which is more than a factor of thirty above the broad-band noise observed with no wiggler.

Detailed results of our measurements will be found in Appendix 1.

2. MILLIMETER WAVE EMISSION FROM A ROTATING ELECTRON RING IN A RIPPLED MAGNETIC FIELD

There have been many theoretical[1] and experimental[2] studies of free electron lasers (FEL's) in linear geometry with spatially periodic transverse[1,2] or longitudinal [3-6] magnetic wiggler fields. Such configurations have gain limitations imposed by the finite length of the interaction region. Recently, a novel circular version of the free electron laser has been explored both theoretically[7,8,9] and experimentally[10] in which a rotating, relativistic electron stream is subjected to an azimuthally periodic wiggler field. The potential advantages of circular FEL's as compared with the conventional linear form are several. First, the beam circulates continuously through the wiggler field resulting in a long effective interaction region. Secondly, because of the recirculation of the growing electromagnetic wave, the device provides its own internal feedback, and is in essence an oscillator rather than an amplifier, as is the case in linear FEL's. And thirdly, because the electron motion is primarily circular the system[10] is very compact.

There are several ways of producing a rotating relativistic electron stream. One is to subject the electrons to orthogonal electric and magnetic fields as is typical in magnetron-like devices. Here, the electrons undergo a $\vec{v}(r)=\vec{E}_0(r)\times\vec{B}_0/|B_0|^2$ drift in a radial electric field $\hat{r}E_0(r)$ and a uniform axial magnetic field $\hat{z}B_0$. Addition of an azimuthally periodic magnetic field $\vec{B}_w(\theta,r)$ then results in a circular FEL. This scheme has been explored previously,[7,8,10] and though the experimental results[10] are encouraging, it may have a potential drawback in that the electron velocity $v(r)$ varies with radial distance r. This velocity shear may lead to degradation of the spectral purity of the emitted electromagnetic radiation, and a reduction in gain and efficiency of the device.

In this letter we describe initial experiments on a circular FEL which uses a monoenergetic rotating electron ring and thereby circumvents the problem of velocity shear mentioned above. Moreover, in the device discussed below one has better control over the circulating current than in a magnetron-like scheme where the anode-cathode gap is part[10] of the magnetic wiggler interaction region.

A high quality (energy spread $\lesssim$ 1%) rotating electron ring is produced by injecting a hollow nonrotating beam into a narrow magnetic cusp.[11,12] The hollow beam is generated by field emission from an annular graphite cathode energized by a pulsed, high voltage, high current accelerator (2MV, 20kA, 30ns). The resulting rotating electron ring is guided downstream from the cusp by a uniform axial magnetic field of $\sim$1.4kG. The ring is 6cm in radius, has a duration of $\sim$5ns, and carries an axial current of $\sim$1.5kA. The electron rotation velocity $v_\theta \simeq 0.96c$, and the electron axial velocity $v_z \simeq 0.2c$. Thus, in the absence of the wiggler magnetic field, the electron orbits form fairly tight helices.

A schematic of the device is illustrated in Fig. 1. It comprises two smooth coaxial stainless steel cylinders of radii r_0=6.58cm and r_i=5.25cm, respectively. The electron ring propagates within the gap formed by the two cylinders. Superimposed on the axial guiding magnetic field is an azimuthally periodic magnetic wiggler field $\vec{B}_w$, which, near the center of the gap, is primarily[10] radial and is thus transverse to the electron flow velocity, as is the case in conventional linear free electron lasers. A single particle computer simulation program has been generated for the purpose of studying the electron motion in the combined axial and wiggler magnetic fields. We see from Fig 2 that the trajectory is not perturbed too strongly: it remains quasi-helical, the radial displacements are small, and the electron does not strike the cylinder walls.

In our device, the wiggler magnetic field is produced by an assembly of 384 samarium-cobalt bar magnets,[10,13] 0.40×0.40×4.8cm, each having a residual induction of ∿9.0kG. The magnets are positioned behind the grounded stainless steel cylinders and held in place in grooved aluminum holders. To achieve a given periodicity ℓ, the dipole axes of the magnets are arranged as illustrated in Fig. 3. The lower part of the figure shows a Hall-probe measurement of the radial component of the wiggler field at the center of the vacuum gap. The measured field amplitude equals 1.31kG. The axial length of the wiggler is 20 cm. This is achieved by stacking end-to-end four rows of bar magnets. At the present time, all of the radiation measurements described below were made with a wiggler having 6 spatial periods (N) and a periodicity ℓ=6.28cm. Shorter periodicities are expected to give radiation at frequencies which lie above the range of our detection equipment.

To estimate the radiation frequency we assume that in the presence of the wiggler, the electrons experience a ponderomotive force which causes electron bunching in the θ direction. When the θ-directed phase velocity $\omega/(k_w + k_\theta)$ of this space charge wave is slightly below the electron velocity v_θ, energy can be given up to the electromagnetic wave. Here $k_w = N/r = 2\pi/\ell$, ω is the radiation frequency; $k_\theta = m/r$ is the radiation wavenumber with m as the mode number of a transverse magnetic (TM) mode of the coaxial waveguide and $r \simeq (r_o + r_i)/2$. Near cutoff $(k_z \to 0)$, one obtains the familiar FEL formula,[1,2]

$$\omega \simeq (1 + \beta_\theta)\beta_\theta \gamma^2 k_w c/K \quad . \tag{1}$$

Here $\beta_\theta = v_\theta/c$, $\gamma = 1 + eV/m_o c^2$ with V as the beam voltage; $\Omega_w = eB_{ow}/m_o$ is the non-relativistic cyclotron frequency in the wiggler field of amplitude B_{ow}, and $K = 1 + (\Omega_w/k_o c)^2$.

The radiation generated in the interaction region is allowed to leak out

from the gap formed by the two coaxial cylinders. It is received by means of a small horn antenna, and is guided through various waveguide cut-off filters to a crystal detector where it is rectified and displayed on a fast oscilloscope. Figure 4c illustrates the time history of a typical radiation burst at frequencies above 91GHz as measured with a T-band (91-170GHz) filter. When the magnetic wiggler field is turned off (by removing the samarium-cobalt magnets from their grooved aluminum cylinders) the emitted power falls to a level too small to be distinguished from background noise (Fig 4d). We thus conclude that the observed radiation is produced only in the presence of the wiggler field.

We have as yet not addressed the problem how best to couple out the available radiation. Our horn antenna merely probes the radiation field and receives only a small fraction of the available power. Using the crystal calibration of our detector, the total power radiated from the device at frequencies above 91GHz is estimated to be no smaller than 200kW. Inserting experimental parameters into Eq. (1) yields a radiation frequency $\omega/2\pi \approx 143$GHz. But, we have not yet measured the spectrum.

In addition to the T-band (91-170GHz) range of frequencies, we also explored emission at lower frequencies, from 21GHz and up. Here we find that some emission occurs even in the absence of the wiggler magnetic field. The cause of this radiation is the negative mass instability.[14-17] However, as a result of the proximity[18] of the two grounded, concentric metal cylinders the level of this radiation is greatly reduced compared to that observed in earlier work[14,15] on the negative mass instability, where the conducting boundaries were not in such close proximity to the beam. When the wiggler magnetic field is introduced the level of the low frequency emission remains either unchanged or in some cases, is diminished. This shows that the pres-

ence of the wiggler field does not enhance the negative mass instability, which has been a worrisome possibility.

In conclusion, we have observed radiation in the millimeter wavelength range ($\lambda < 3.3$mm) from a novel type of circular FEL which uses a high quality, high current relativistic electron ring rotating in an azimuthally periodic wiggler magnetic field. The emitted power attributed to the FEL instability is at least 200kW. Spectral measurement using a calibrated microwave grating spectrometer[10,19] will be carried out in the near future. In addit ., by rearranging the magnets as illustrated in Fig. 3, we will be able to sh en the wiggler periodicity ℓ and thereby study emission at wavelengths rangir from 0.05 to 1.0mm.

3. RELATIVISTIC MAGNETRON--AN INVERTED MULTIRESONATOR SYSTEM

The relativistic magnetron operating in the 400kV range is capable of producing microwave bursts on the order of 0.5GW at 12% efficiency. Scaling to higher voltage (1.0MV) results in increased power (0.8GW); however, the overall efficiency is reduced due to the presence of a large axial, noninteracting current. This problem is difficult to overcome at high field strengths in a conventional magnetron design with the cathode placed coaxially inside the anode. A solution to this problem is to operate in an inverted geometry with the cathode located outside the anode. In this configuration, an electron emitted from the cathode that flows axially returns to the cathode with no loss of current. This property of the inverted magnetron has been investigated experimentally.

The operation of an oscillating magnetron in the inverted geometry requires a nonconventional method for extracting the RF power since there intervenes a dense space charge cloud between the external world and the RF resonators. One technique is to build a large radius tube with many vanes (N>20).

Here the power is extracted from the backs of the resonators, is stored in a center cavity, and then coupled out the front. Alternatively, it may be possible to extract the RF fields with magnetic coupling through an iris in the outer cathode surface. This allows for a compact design with a small number of anode vanes. We have chosen the latter extraction technique. We have successfully operated the inverted magnetron, and its characteristics are: magnetic field = 6.86kG; voltage = 1.73MV; current = 8.4kA; frequency = 3.68GHz; microwave power = 400MW.

The detailed results of these studies will be found in Appendix 2.

REFERENCES

1. N.M. Kroll and W.A. McMullin, Phys. Rev. A17, 300 (1978); P. Sprangle and R.A. Smith, Phys. Rev. A21, 293 (1980) and references therein.

2. P.A. Sprangle, R.A. Smith, and V.L. Granatstein in "Infrared and Submillimeter Waves", K. Button editor (Academic Press, N.Y. 1979) Vol. 1, page 279 and references therein.

3. W.A. McMullin and G. Bekefi, Appl. Phys. Lett. 39, 845 (1981).

4. W.A. McMullin and G. Bekefi, Phys. Rev. A25, 1826 (1982).

5. R.C. Davidson and W.A. McMullin, Phys. Rev. A26, 1997 (1982).

6. R.C. Davidson and W.A. McMullin, Phys. Fluids 26, 840 (1983).

7. G. Bekefi, Appl. Phys. Lett. 40, 578 (1982).

8. R.D. Estes, A. Palevsky, and A.T. Drobot, Bull. Am. Phys. Soc. 27, 1075 (1982); also R.E. Shefer, G. Bekefi, R.D. Estes, C-L. Chang, E. Ott, T.M. Antonsen, and A. T. Drobot, Proceedings Fifth International Topical Conference High Power Electron and Ion-Beam Research and Technology, San Francisco 1983.

9. R. C. Davidson and W.A. McMullin, Massachusetts Institute of Technology, Cambridge, Massachusetts, Plasma Fusion Center Report No. PFC/JA-82-33 (1982).

10. G. Bekefi, R.E. Shefer, and B.D. Nevins, Massachusetts Institute of Technology, Cambridge, Massachusetts, Plasma Fusion Center Report No. PFC/JA-83-3 (1983); also Lasers '82, Society for Optical and Quantum Electronics, SOQUE (1982) (to be published).

11. M.J. Rhee and W. W. Destler, Phys. Fluids 17, 1574 (1974).

12. W.W. Destler, P.K. Misra, and M.J. Rhee, Phys. Fluids 18, 1820 (1975).

13. K. Halbach, Lawrence Berkeley Laboratory, University of California Accelerator and Fusion Research Division Repor+ No. LBL11393, August 1980; also IEEE Trans. Nucl. Sci. NS-26, 3882 (1979).

14. W.W. Destler, H. Romero, C.D. Striffler, R.L. Weiler, and W. Namkung, J. Appl. Phys. 52, 2740 (1981).

15. W.W. Destler, D.W. Hudgings, M.J. Rhee, S. Kawasaki, and V.L. Granatstein, J. Appl. Phys. 48, 3291 (1977).

16. H. Uhm and R.C. Davidson, J. Appl. Phys. 49, 593 (1978).

17. Y. Goren, H. Uhm, and R.C. Davidson, J. Appl. Phys. 49, 3789 (1978).

18. L.J. Laslett, IEEE Trans. N.S.20, 271 (1973).

19. J.A. Pasour and S.P. Schlesinger, Rev. Scient. Instr. 48, 1355 (1977); also R.E. Shefer, Ph.D Thesis, Department of Physics, M.I.T. (1981). (Unpublished).

FIGURE CAPTIONS

Fig. 1. General experimental configuration.

Fig. 2. Calculated particle orbits in the r-θ and r-z planes for an electron injected with v_z=0.20c, v_θ=0.96c into the interaction space with (a) B_{0z}=1.4kG, B_{0w}=0, and (b) B_{0z}=1.4kG, B_{0w}=1.3kG.

Fig. 3. Arrangement of bar magnets (top); Hall probe measurement of the wiggler field at a radial position r=5.92cm, as a function of azimuthal angle (bottom).

Fig. 4. Oscilloscope waveforms of (a) diode voltage, (b) axial current collected by a 2.24mm^2 collector located in the center of the interaction region, (c) microwave signal in T-band (91-170GHz) with wiggler magnets, and (d) microwave signal in T-band without wiggler magnets.

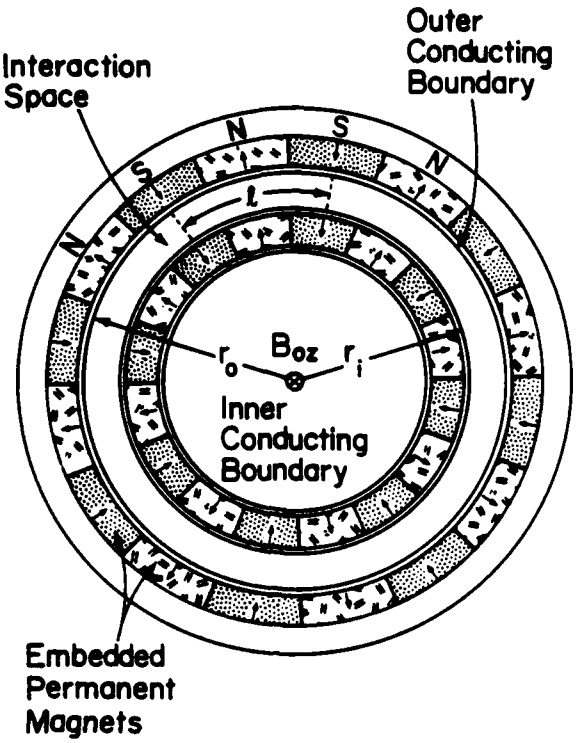
Interaction Space
Outer Conducting Boundary
N
S
N
S
N
l
r_o
B_{oz}
r_i
Inner Conducting Boundary
Embedded Permanent Magnets

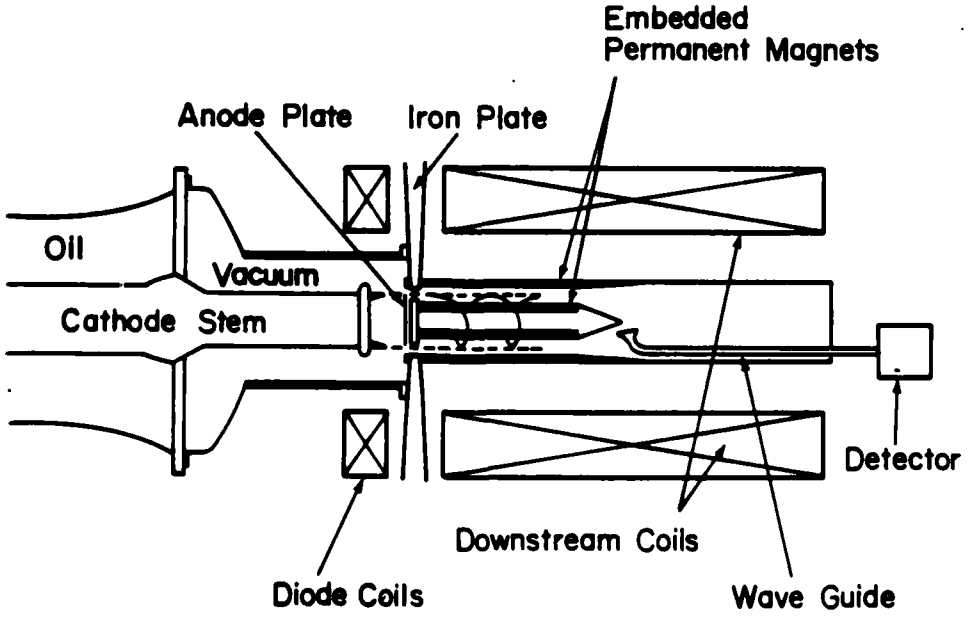
Embedded Permanent Magnets
Anode Plate
Iron Plate
Oil
Vacuum
Cathode Stem
Detector
Downstream Coils
Diode Coils
Wave Guide

Fig. 1

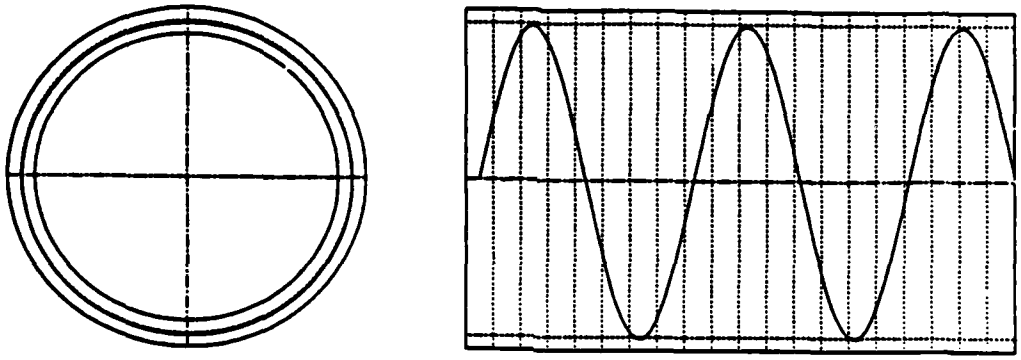

(a)

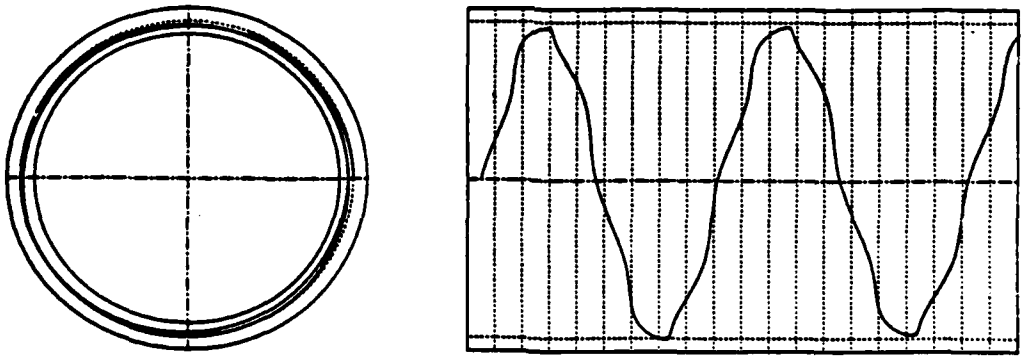

(b)

Fig. 2

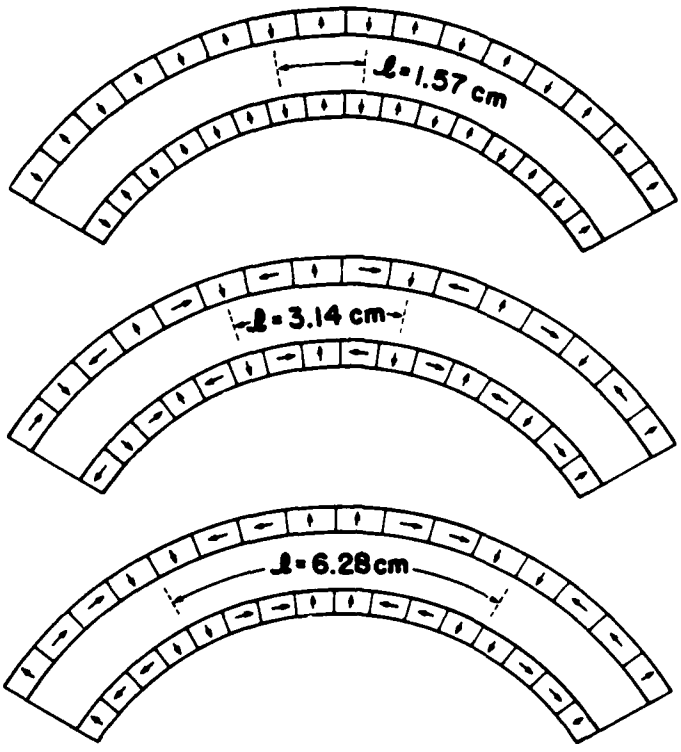
ℓ = 1.57 cm
ℓ = 3.14 cm
ℓ = 6.28 cm

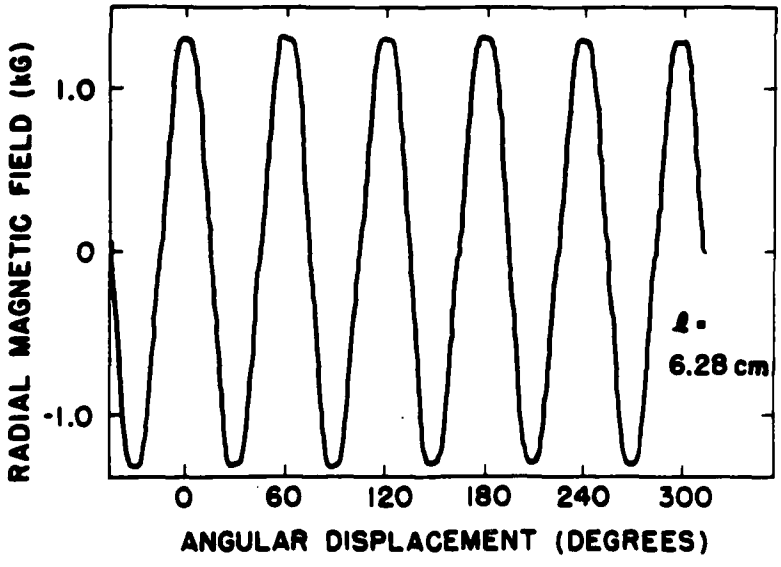
RADIAL MAGNETIC FIELD (kG)
1.0
0
-1.0
0
60
120
180
240
300
ANGULAR DISPLACEMENT (DEGREES)
ℓ = 6.28 cm

Fig. 3

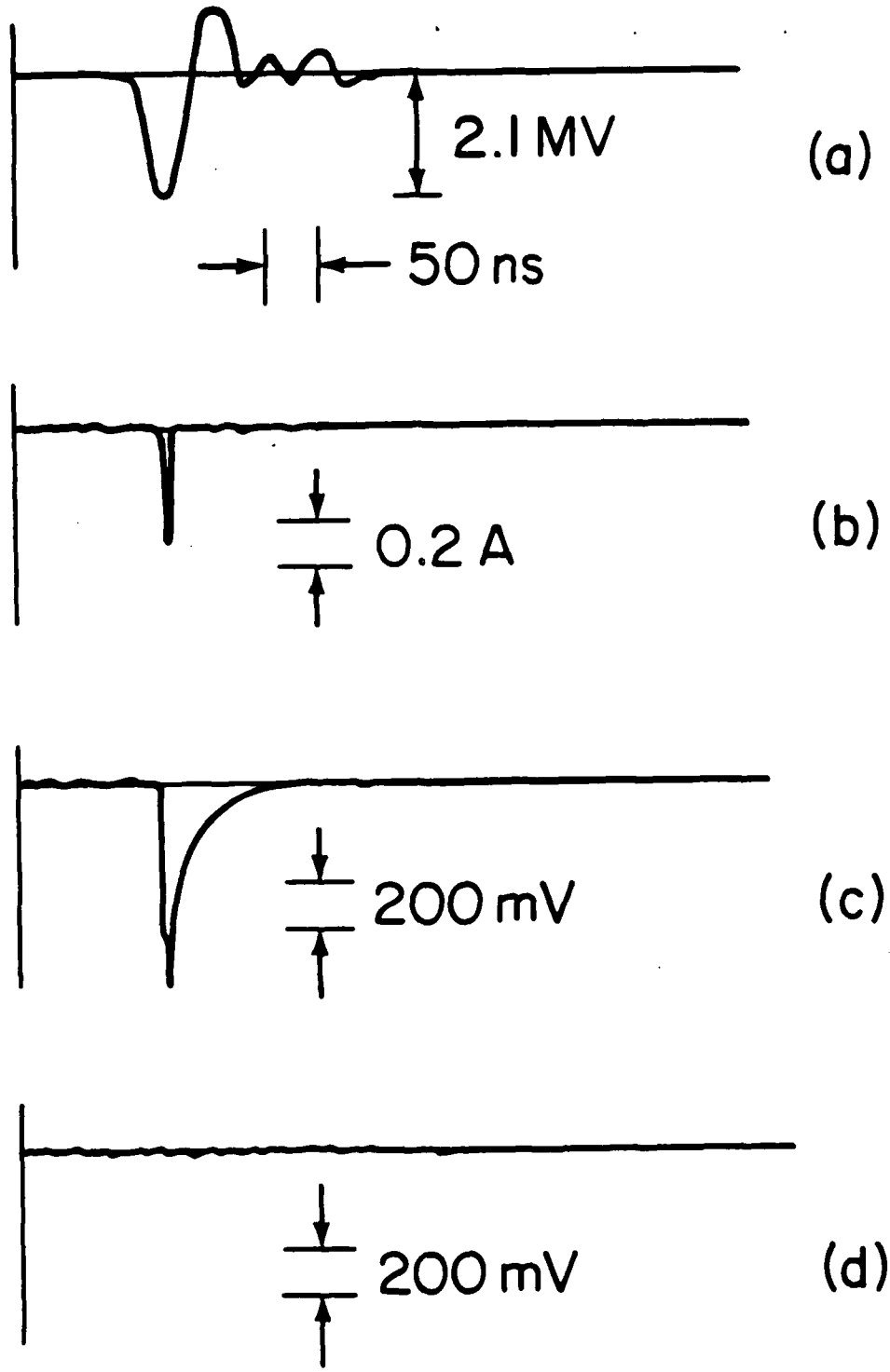

Fig. 4

APPENDIX 1

REPRINTED FROM PROCEEDINGS OF THE INTERNATIONAL CONFERENCE ON LASERS '82, DECEMBER 13-17, 1982 Appendix 1

RADIATION MEASUREMENTS FROM A RIPPLED-FIELD MAGNETRON (CROSSED-FIELD FEL)

G. Bekefi, R.E. Shefer, and B.D. Nevins

Department of Physics and Research Laboratory of Electronics
Massachusetts Institute of Technology
Cambridge, Massachusetts 02139

Abstract

We report measurements of millimeter wave emission from a rippled-field magnetron (crossed-field FEL). This is a novel source of coherent radiation in which electrons move in quasi-circular orbits under the combined action of a radial electric field, a uniform axial magnetic field and an azimuthally periodic wiggler magnetic field. We observe ∿300kW of RF power in a spectral line whose frequency can be continuously varied from ∿32 to ∿45 GHz by varying the axial magnetic field.

I. Introduction

The rippled-field magnetron[1] (or crossed-field FEL) is a novel source of coherent radiation in the millimeter and submillimeter wavelength ranges. The configuration is a hybrid between a smooth-bore magnetron[2] and a free electron laser.[3] Its similarity to the magnetron lies in the fact that the electrons are subjected to orthogonal electric and magnetic fields causing them to undergo a $\vec{v} = \vec{E}\times\vec{B}/B^2$ drift. Its similarity to the free electron laser comes from the fact that the electrons are also subjected to a spatially periodic wiggler magnetic field $\vec{B}_w$ which imposes upon them an undulatory motion.

The device is illustrated schematically in Fig. 1. It comprises a smooth cylindrical cathode of radius r_c enclosing a smooth coaxial cylindrical anode of radius r_a. The electrons, emitted from the cathode by field emission, are subjected simultaneously to two quasi-steady fields acting at right angles to one another: a uniform, axial magnetic field B_{0z} produced by magnetic coils, and a radial electric field $E_{0r}(r)$ generated by applying a voltage V between the electrodes. In the absence of the wiggler field, a space-charge cloud forms, partially filling the interaction gap ($r_c - r_a$); the electrons undergo azimuthal rotation having a sheared, radially dependent velocity $v_\theta = E_{0r}(r)/B_{0z}$. To achieve this "Brillouin flow equilibrium," the strength of the magnetic field must exceed the critical field for "magnetic insulation", given by[2]

$$B_{0c} = (m_0 c/ed_e)(\gamma_0^2 - 1)^{\frac{1}{2}}, \tag{1}$$

where e and m_0 are the electron charge and rest mass, respectively, $\gamma_0 = 1+(eV/m_0c^2)$ and $d_e = (r_c-r_a)/2r_a$ is the effective cathode-anode gap width.

Superimposed on the $\vec{E}_0$ and $\vec{B}_0$ fields is an azimuthally periodic magnetic wiggler field $\vec{B}_w$, which perturbs the Brillouin flow of the electron stream. Subject to the requirement that $\nabla\cdot\vec{B}_w = \nabla\times\vec{B}_w = 0$, the field in the vacuum gap between the cathode and anode is calculated to be,

$$\vec{B}_w = \hat{r}\,\frac{B_{0w}}{2}\cos(N\theta)\left[\left(\frac{r}{r_c}\right)^{N-1} + \left(\frac{r_a}{r}\right)^{N+1}\right]\left[\frac{r_c}{r_a}\right]^{(N^2-1)/2N}$$
$$- \hat{\theta}\,\frac{B_{0w}}{2}\sin(N\theta)\left[\left(\frac{r}{r_c}\right)^{N-1} - \left(\frac{r_a}{r}\right)^{N+1}\right]\left[\frac{r_c}{r_a}\right]^{(N^2-1)/2N} \tag{2}$$

where $\hat{r}$ and $\hat{\theta}$ are unit vectors in the radial and azimuthal directions, respectively. $N = \pi(r_c+r_a)/\ell$ is the number of spatial periods and ℓ is the linear periodicity defined midway in the gap. B_{0w} is the amplitude of the radial component of field at a distance $r = r_{c}^{N-1}r_{a}^{N+1}$ ($= r_N$) where the azimuthal field component vanishes (which is roughly midway between the cathode and anode). We see that near the center of the gap the wiggler field is primarily radial and is thus transverse to the electron flow velocity $\vec{v} = \hat{\theta}\,v_\theta$, as is the case in conventional free electron lasers. The undulatory force $-ev_\theta B_w$ is along the $\hat{r}$

axis.

In our device, the wiggler magnetic field is produced by an assembly of samarium-cobalt bar magnets. The placement of the magnets and the electrode configuration are illustrated in the photograph of Fig. 2. The magnets are positioned behind smooth stainless steel electrodes and held in place in grooved aluminum cylinders. Once the system is assembled, the inner electrode (anode) is connected to the positive terminal of the pulsed, high voltage accelerator. The outer field-emission cathode is grounded. Table I gives a summary of the diode dimensions and experimental parameters, and Table II gives data concerning the permanent magnet system.

TABLE I. Summary of operating parameters of the rippled-field magnetron.

Radius of cathode	5.22 cm
Radius of anode	4.43 cm
Length of anode	6.0 cm
Voltage	0.7-1.4 MV
Current	1-20 kA
Pulse length	30 ns
Axial magnetic field	6-15 kG

TABLE II. Summary of the samarium-cobalt bar magnet assembly.

Number of magnets = 96
Dimensions = 0.40×0.40×4.8 cm
Residual induction, B_r = 9.0 kG

Periodicity ℓ (cm)	N	Field Amplitude B_{ow} (kG)
1.26	24	0.68
2.53	12	1.96
5.06	6	2.26

To achieve the different periodicities ℓ given in Table II above, the dipole axes of the magnets are arranged as illustrated in Fig. 3. Because the magnets are discrete, harmonics of the fundamental period $\cos(N\theta)$ are present. However, use of four or eight magnets per period as shown in the second and third diagrams greatly reduces the harmonic content: all even harmonics are absent and the third harmonic also vanishes. As a result, the magnetic field closely resembles that given by Eq. (2). Figure 4 shows a Hall-probe measurement of the radial component of the wiggler field at the center of the cathode-anode gap. Figure 5 gives a computer generated field plot in x,y coordinates. For small gaps such that $(r_c-r_a)\ll r_c$, which is the case in our system, the x,y plot is a good approximation to the actual cylindrical, r,θ, configuration. We see that at the center of the gap, the field is purely transverse (radial); however, at the electrode surfaces, the transverse (radial) and longitudinal (azimuthal) field components are of comparable magnitude. This is of course borne out by Eq. (2).

II. Experiments

Figures 6 and 7 show an overall view of the experimental arrangement. The electric field between cathode and anode is provided by the Physics International Pulserad 110A high voltage facility. The axial magnetic field is generated by two pulsed magnetic field coils surrounding, and coaxial with, the cylindrical electrodes. Typical current-voltage charac-

teristics of the system as a function of the axial magnetic field are shown in Fig. 8. In all cases the magnetic field exceeds the critical field given by Eq. (1).

The radiation generated in the rippled-field magnetron is allowed leak out through the Pyrex window seen in Figs. 6 and 7. We point out that we have as yet not addressed the problem how best to couple out the available radiation. We believe that only a fraction of the radiation generated reaches our externally placed diagnostics. The radiation leaving the Pyrex window in a given direction is received with a horn antenna and rectified in a calibrated crystal detector. To obtain the total emitted power[2] in a given microwave frequency band, we make an angular scan of the radiation pattern of the transmitter, derive its gain and use the familiar radar formula.[2]

The frequency spectra are measured in one of two ways, by means of solid state or waveguide dispersive lines[2] and by a millimeter wave grating spectrometer[5] (shown in Figs. 6 and 7). A dispersive line gives the spectrum in a single firing of the accelerator, but has a rather poor spectral resolution. The grating spectrometer has much better resolution and is used for final, detailed measurements. However, since the spectra must be assembled from successive shots, its use is not practical when the frequency fluctuates, as is sometimes the case. Table III summarizes the frequency bands explored in our studies. However, we shall restrict further discussions to the 26-60GHz range of frequencies because in this range only do we observe a clear narrow spectral line which is unmistakably associated with the presence of the wiggler magnetic field. In the other two bands listed in Table III we observe lower level radiation not clearly connected with the presence or absence of the wiggler. This emission is probably of the same origin as that seen in earlier studies of the smooth-bore magnetron.

TABLE III. Frequency range of spectral studies

Frequency band (GHz)	Method
2 - 4	Solid state dispersive line.
7 - 12	Waveguide dispersive line.
26 - 60	Grating spectrometer; waveguide dispersive line.

Figure 9 shows the total radiated power in the 26-40GHz frequency band, as a function of the axial magnetic field, for a wiggler having a periodicity ℓ=2.53cm(N=12) and an amplitude $B_{\sim w}$=1.96kG. The peak emitted power exceeds 300kW. When the wiggler is turned off (by removing the samarium-cobalt magnets from their grooved aluminum cylinders), the emitted power is seen to fall by more than a factor of 20. When the amplitude of the wiggler field is reduced from 1.96kG to 0.98kG (not shown in the figure), the emitted power is reduced by approximately a factor of two. The reduction in $B_{\sim w}$, without a change in the period ℓ, is accomplished by removing the azimuthally directed magnets shown in the second diagram of Fig. 3.

Spectral characteristics of the emitted radiation, obtained with the grating spectrometer are illustrated in Fig. 10. The measured line width at the half power points is ~2.2 GHz (the instrument line width is ~1.0GHz). The lower part of Fig. 10 shows that in the absence of the wiggler, the level of radiation has fallen by more than three orders of magnitude; the emission is broad-band and shows no narrow spectral features.

The radiation frequency of the spectral line shown in Fig. 10 varies linearly with the strength of the axial magnetic field. This continuous frequency tuning from 32GHz to 45GHz is illustrated in Fig. 11. At frequencies below 30GHz (magnetic fields below 5kG) the emission becomes erratic, probably due to the fact that the corresponding axial magnetic field approaches too closely the critical field of Eq. (1). At frequencies above 45GHz the amplitude of the spectral line becomes very small. Shot-to-shot reproducibility of the emission is good over the entire frequency range shown in the figure. Thus, detailed grating spectrometer measurements are possible, and these are shown as open circles. The solid dots denote measurements made with a Ka band waveguide dispersive line. The straight line shown in Fig. 11 represents a least squares fit to the experimental data and is of the form,

$$\frac{}{2} \text{ (GHz)} = 9.4 + 4.0\ B_z\text{(kG)} \qquad \text{for} \quad = 2.53\text{cm} \tag{3}$$

No deterioration of the spectral line profile occurs over the frequency range of Fig. 11; the experimental line width is less than 2GHz.

Changing the period ℓ of the wiggler changes the radiation frequency ω. Figure 12 shows the tuning curve for ℓ=5.06cm(N=6), and a wiggler amplitude B_{0w}=2.26kG. In the measurements the frequency spectra are obtained with the Ka band dispersive line; it appears that shot-to-shot frequency fluctuations prevent use of the grating spectrometer. No line emission occurs at frequencies below ~40GHz. The straight line shown in Fig. 12 is a least squares fit to the data, and is of the form,

$$\frac{\omega}{2\pi}\,(\mathrm{GHz}) = 5.4 + 3.9\,B_z(\mathrm{GHz}) \qquad \text{for } \ell = 5.06\mathrm{cm} \tag{4}$$

It is noteworthy that for a given value of B_z, the radiation frequency is higher for a wiggler of shorter period ℓ, a fact which will be discussed in section III.

III. Discussion

We have observed intense (~300kW), narrow band (≤2GHz) radiation in the millimeter wavelength range (7-9mm). The available radiation is probably much in excess of what we observe. The problem of designing an efficient power extraction circuit has not been addressed yet. Such a design requires better knowledge of the RF mode structure and the physics of the emission mechanism than are presently available.

Dependence of the radiation frequency ω on the externally applied axial magnetic field B_z, and on the wiggler periodicity ℓ suggests that one is dealing with a Doppler upshifted cyclotron mode[6]

$$\omega = (k + k_w)v + \frac{c}{\gamma} \tag{5}$$

coupled to an electromagnetic wave

$$\omega = kc \tag{6}$$

circulating in the cathode-anode gap. Here ω and k are the radiation frequency and azimuthal wave number, respectively; $k_w=2\pi/\ell$ is the wiggler wave number; v is the azimuthal velocity of an electron interacting with the wave, and $\gamma=(1-(v/c)^2)^{-\frac{1}{2}}$. $\Omega_c=eB_z/m_0$ is the nonrelativistic electron cyclotron frequency associated with the axial magnetic field; and e and m_0 are the electron charge and rest mass, respectively. Eliminating k between Eqs. (5) and (6) yields

$$\omega = (1 + \beta)\beta\gamma^2 k_w c + (1 + \beta)\Omega_c \tag{7}$$

where $\beta = v/c$.

We see that the empirical Eqs. (3) and (4) have the same structure as Eq. (7). The radiation frequency varies linearly with magnetic field B_z, and for a given B_z, increases with decreasing periodicity ℓ. A quantitative comparison can be made as follows. Determine β by equating the second term of Eq. (7) to the second term of Eqs. (3) or (4). Using this value of β compute the first term of Eq. (7) and compare it with the first term of Eqs. (3) or (4). Table IV summarizes the results.

TABLE IV. Comparison of coefficients a and b in the equation $\omega/2\pi$(GHz) = a + bB_z(kG).

	ℓ = 2.53cm β = 0.44	ℓ = 5.06cm β = 0.39
Experiment (Eq. (3) or (4))	$\frac{\omega}{2\pi}$ = 9.4+4.0B_z	$\frac{\omega}{2\pi}$ = 5.4+3.9B_z
Equation (7)	$\frac{\omega}{2\pi}$ = 9.4+4.0B_z	$\frac{\omega}{2\pi}$ = 3.8+3.9B_z

There is remarkably good agreement between Eq. (7) and the empirical Eq. (3) for the 2.53cm period wiggler. The agreement is somewhat worse for the 5.06cm wiggler. However, in the latter case, there is fairly large scatter in the experimental data as seen in Fig. 12. We note that the values of β derived above are less than the maximum β that can be imparted by the applied electric and magnetic fields. This implies that only electrons close to the cathode participate in the wave-particle interaction (the velocity $\bar{v} = E_r(r)/B_z$ is sheared; it is zero at the cathode and increases roughly linearly with distance towards the anode). The computed values of β given in Table IV are constant, independent of the strength of the axial magnetic field B_z. This is only possible if the electric field E_r varies such that the ratio E_r/B_z = constant, a fact which is borne out by the voltage versus B_z plot of Fig. 8.

The theoretical understanding of the observed emission mechanism is far from complete, and the validity of Eq. (7) for the radiation frequency must not be overemphasized. Equation (7) is derived[6] under assumptions not really applicable to the experimental device. The single particle computations neglect space charge effects, and the electrons are injected into the cathode-anode gap with finite velocity, rather than being born in situ at the cathode. Finally, the wiggler magnetic field is taken to be purely radial and this neglects the strong azimuthal field component at the cathode and anode surfaces (Eq. (2)). Indeed, with the above theoretical assumptions, the mode represented by Eqs. (5), (6), and (7) is stable, that is, the imaginary part of the complex frequency is zero. We expect to obtain a better understanding of the observed phenomena from a particle simulation code.[7] This is a fully relativistic particle-in-cell code used in previous studies of the relativistic magnetron.[8] Preliminary computer simulations indicate that a large fraction of electrons emitted at the cathode do not in fact circulate but travel directly to the anode. A temporal space charge density modulation occurs accompanied by an azimuthally periodic density variation. An understanding of the emission mechanism will have to take cognizance of the effect of these space charge fields on the dynamics of the circulating component of the electron stream.

Acknowledgements

This work was supported in part by the United States Air Force Office of Scientific Research, and in part by the Department of the Air Force Aeronautical Systems Division (AFSC).

References

1. G. Bekefi, Appl. Phys. Lett. 40, 578 (1982).
2. T.J. Orzechowski and G. Bekefi, Phys. Fluids 22, 978 (1979); and references therein.
3. N.M. Kroll and W.A. McMullin, Phys. Rev. A17, 300 (1978); P. Sprangle and R.A. Smith, ibid. 21, 293 (1980).
4. K. Halbach, Lawrence Berkeley Laboratory, University of California Accelerator and Fusion Research Division Report No. LBL11393, August 1980.
5. J.A. Pasour and S.P. Schlesinger, Rev. Scient. Instr. 48, 1355 (1977).
6. W.A. McMullin and R.C. Davidson, Bull. Am. Phys. Soc. 27, 1074 (1982).
7. R.D. Estes, A. Palevsky, and A.T. Drobot, Bull. Am. Phys. Soc. 27, 1075 (1982).
8. A. Palevsky, G. Bekefi, and A.T. Drobot, J. Appl. Phys. 52, 4938 (1981).

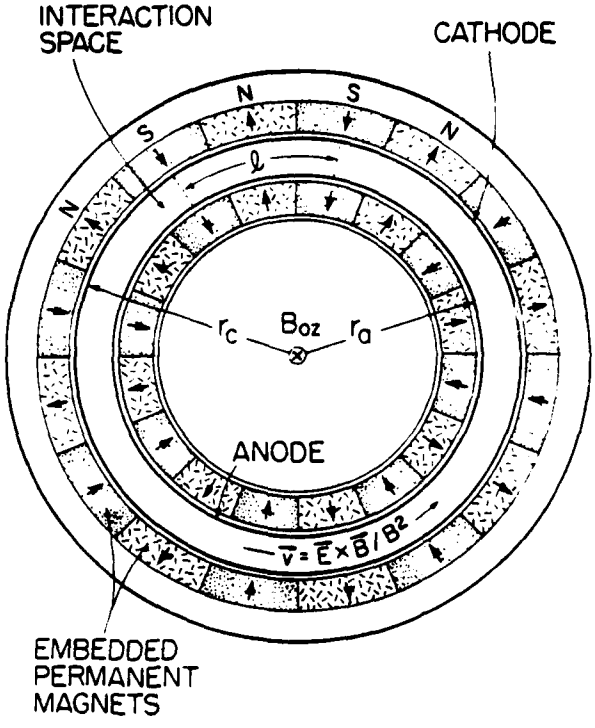

Fig. 1. Schematic diagram of the rippled-field magnetron.

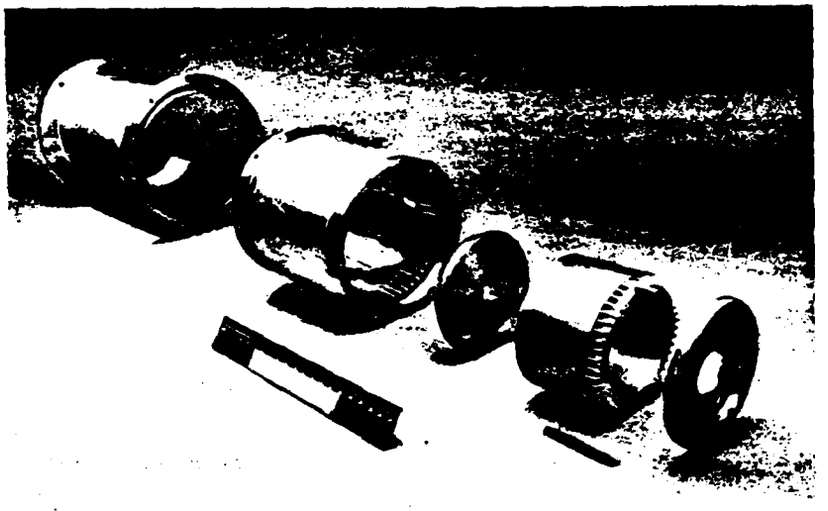

Fig. 2. Photograph of the disassembled rippled-field magnetron, with a samarium-cobalt bar magnet shown in the foreground.

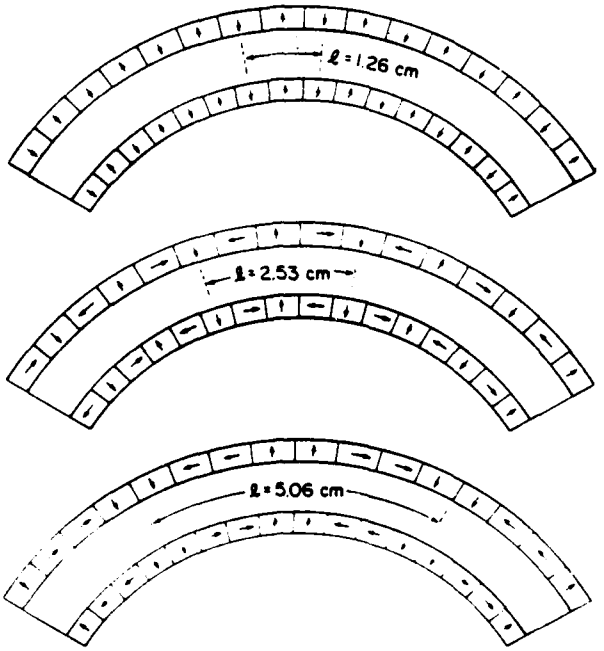

Fig. 3. Arrangement of bar magnets for three different periodicities .

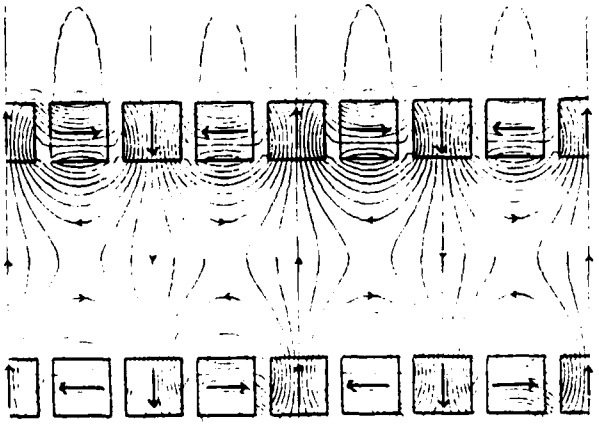

Fig. 5. Computer generated magnetic field plot in the cathode-anode gap of a planar version of the rippled-field magnetron.

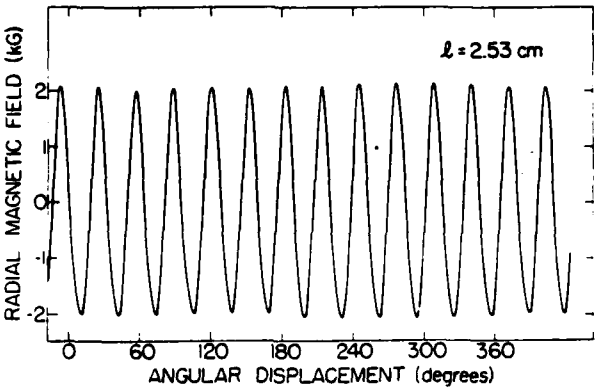

Fig. 4. X-Y recorder output of the radial magnetic field midway in the cathode-anode gap, as a function of azimuthal angle θ.

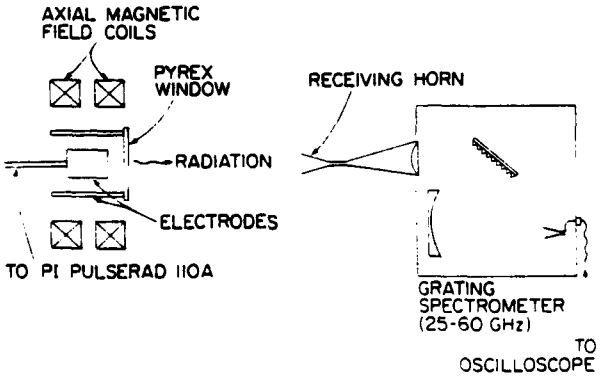

Fig. 6. Experimental arrangement.

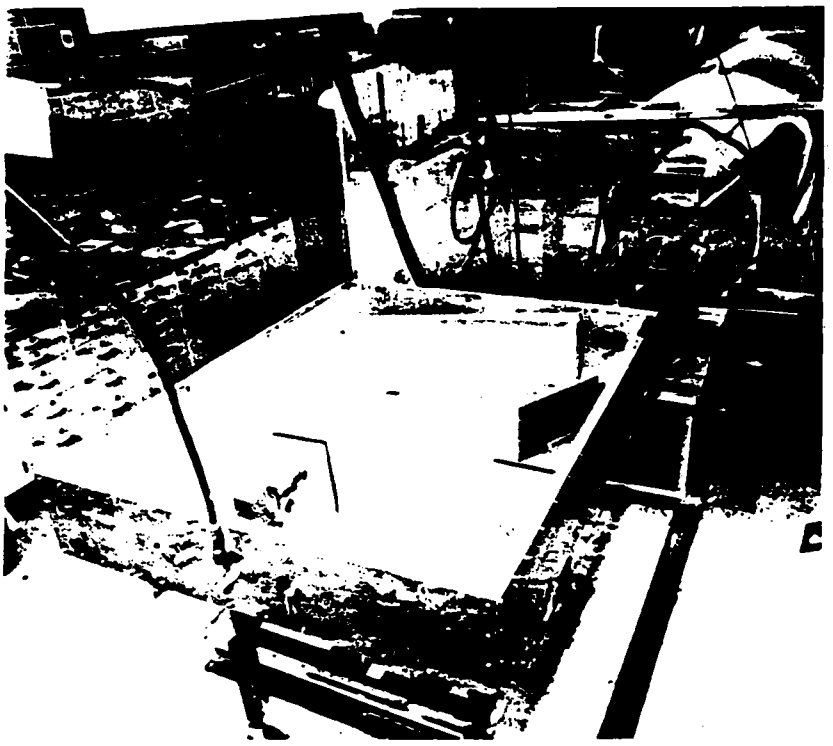

Fig. 7. Photograph of the experimental arrangement showing the glass output window and axial magnetic field coils of the rippled-field magnetron in the background; and the millimeter-wave grating spectrometer in the foreground.

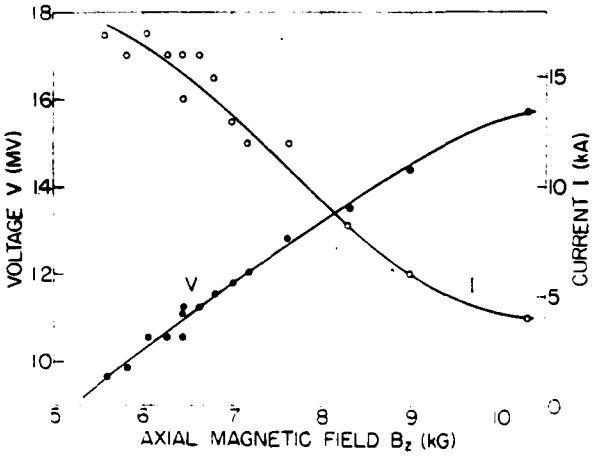

Fig. 8. Current-voltage characteristics of the rippled-field magnetron as a function of the axial magnetic field (B_w=1.96kG, =2.53cm).

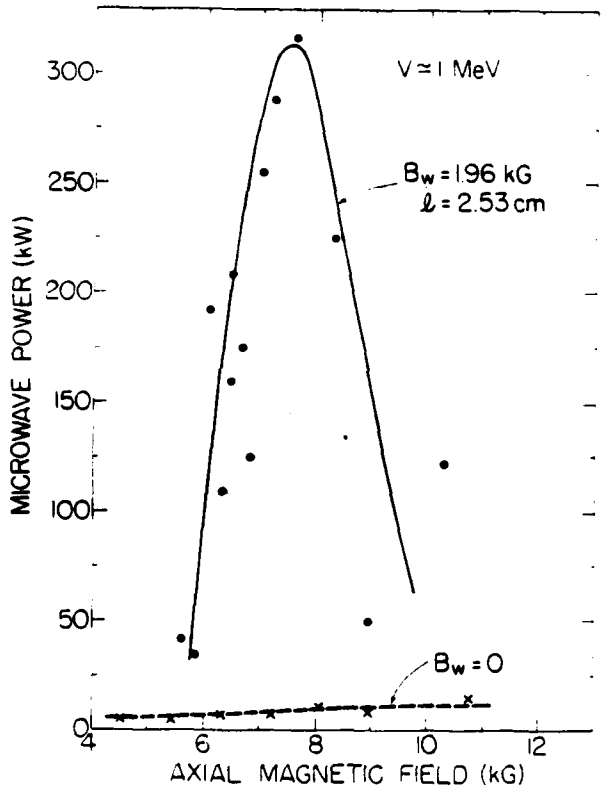

Fig. 9. Radiated power in the 20-40GHz frequency range as a function of the axial magnetic field.

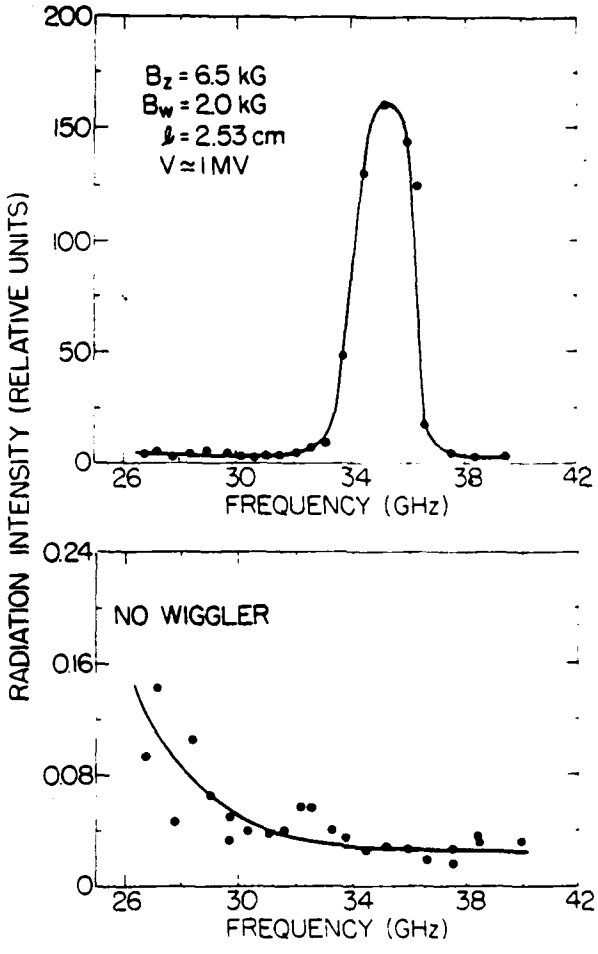

Fig. 10. Emission spectrum in the presence and absence of the magnetic wiggler as measured with the millimeter-wave grating spectrometer.

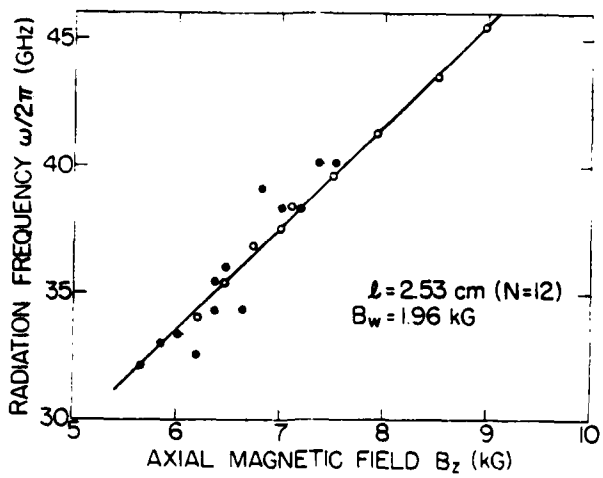

Fig. 11. Radiation frequency as a function of axial magnetic field for the ℓ=2.53cm period wiggler (● dispersive line measurement; 0 grating spectrometer measurements).

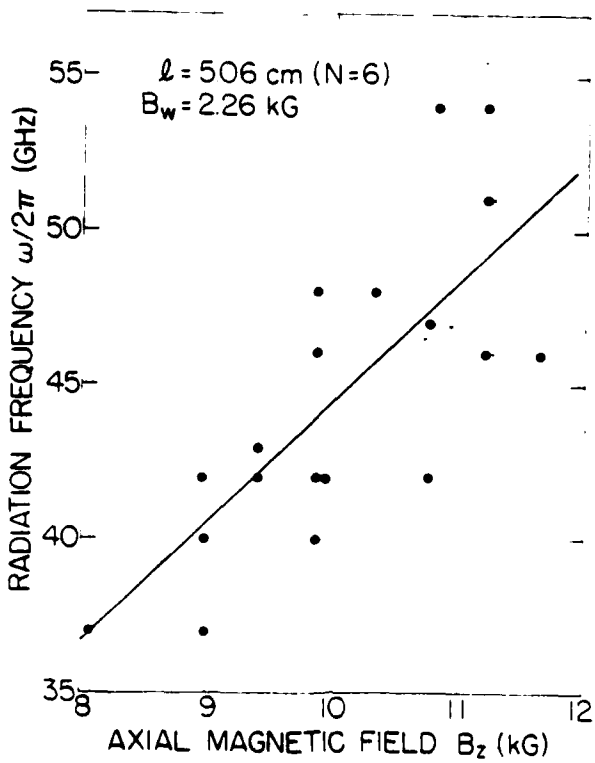

Fig. 12. Radiation frequency as a function of axial magnetic field for ℓ=5.06 cm period wiggler (● dispersive line measurements).

APPENDIX 2

Radiation measurements from an inverted relativistic magnetron

R. A. Close, A. Palevsky, and G. Bekefi
Department of Physics and Research Laboratory of Electronics, Massachusetts Institute of Technology, Cambridge, Massachusetts 02139

(Received 31 January 1983; accepted for publication 30 March 1983)

We report microwave emission measurements from an inverted relativistic magnetron comprising an outer cylindrical field emission cathode and an inner coaxial anode with embedded vane resonators. The magnetron operates in the π mode at a frequency ~ 3.6 GHz, and voltages of 1–2 MV. The rf power is ~ 500 MW.

PACS numbers: 85.10.Ka

I. INTRODUCTION

The magnetron[1,2] is one of the most efficient and rugged devices for generating microwaves at decimeter and centimeter wavelength ranges. Power levels from tens of watts to hundreds of kilowatts can be achieved with conversion efficiencies as high as 80%. In recent years[3–9] a new class of pulsed magnetron devices has come into existence which are capable of extending the existing powers by more than two orders in magnitude. This has resulted in the generation of unprecedented powers in the range of hundreds of megawatts to several gigawatts (albeit at reduced efficiencies of 10%–35%).

In slow-wave systems, efficient conversion of energy from a stream of free electrons to electromagnetic radiation requires near synchronism between the velocity of the electrons and the phase velocity of the wave. In crossed-field devices, of which the magnetron is a typical example, this synchronism occurs between electrons undergoing a $\mathbf{v} = \mathbf{E} \times \mathbf{B}/B^2$ drift in orthogonal electric and magnetic fields, and an electromagnetic wave whose velocity is reduced by a slow-wave structure comprised of a periodic assembly of coupled resonant cavities.

The device is illustrated schematically in Fig. 1. It comprises a smooth cylindrical cathode of radius r_c enclosing a coaxial cylindrical anode of radius r_a. The electrons, emitted from the cathode by field emission[4,10] are subjected simultaneously to two quasisteady fields acting at right angles to one another: a uniform, axial magnetic field B_{oz} produced by magnetic coils, and a radial electric field $E_{or}(r)$ generated by applying a voltage V between the electrodes. As a result, a space-charge cloud forms, partially filling the interaction gap $(r_c - r_a)$; the electrons undergo azimuthal rotation having a sheared, radially dependent velocity $v_\theta = E_{or}(r)/B_{oz}$. To achieve this "Brillouin flow equilibrium," the strength of the magnetic field must exceed the critical field for "magnetic insulation," given by[4,10]

$$B_{oc} = (m_0 c/ed_e)(\gamma_0^2 - 1)^{1/2}, \tag{1}$$

where e and m_0 are the electron charge and rest mass, respectively; $\gamma_0 = 1 + (eV/m_0c^2)$ and $d_e = (r_c^2 - r_a^2)/2r_a$ is the effective cathode–anode gap width.

Embedded in the anode block is a periodic assembly of vane-type resonators[3] whose function is to create slow modes (phase velocity $< c$) with which the circulating electrons can interact. Once the system is assembled, the inner electrode (anode) is connnected to the positive terminal of a pulsed high voltage accelerator. The outer, field emission cathode is grounded. Table I gives a summary of the experimental parameters and dimensions of two tubes (M8 and M10) and Table II gives their (approximate) mode frequencies computed by a method[1,4] described elsewhere.

The eight-vane (M8) and ten-vane (M10) tubes are designed with the view (see Sec. III) of testing two magnetrons radiating at the same π-mode frequencies but having widely different cathode–anode gap widths d. This is achieved by changing the number of vane resonators from eight to ten as the gap width is changed from 1.38 to 0.84 cm, respectively.

It is clear from Fig. 1 that the configuration of the magnetrons under present investigation is inverted compared to the typical magnetron[1–4] which has an outer (grounded) an-

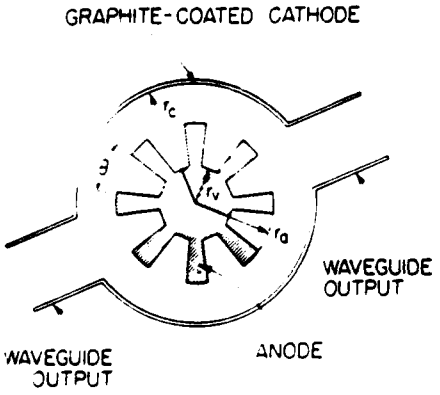

FIG. 1. Schematic diagram of the M8 inverted relativistic magnetron..

TABLE I. Summary of operating parameters of two inverted relativistic magnetrons (the nomenclature is that used in Fig. 1).

Voltage	0.9–2.1 MV
Current	1–14 kA
Pulse length	30 ns
Axial magnetic field	2–6 kG

Quantity		M8 Magnetron	M10 Magnetron
Number of vanes		8	10
Anode radius	r_a	2.92 cm	3.76 cm
Cathode radius	r_c	4.30 cm	4.60 cm
Gap width	d	1.38 cm	0.84 cm
Anode length	L	5.07 cm	4.64 cm
Vane radius	r_v	1.28 cm	2.55 cm
Vane angle	θ	30°	20°

 0021-8979/83/074147-05$02.40

TABLE II. Computed (and measured) mode frequencies of the M8 and M10 inverted magnetrons. Mode designations conform to those used in Refs. 1 and 4.

Mode	Frequency (GHz)	
	M8	M10
Calculated		
1	1.10	< 0.95
2	2.15	1.72
3	3.10	2.48
4	...	3.15
π	3.53	3.69
2π (0)	> 4.7	> 4.7
Measured (cold test)		
π	...	3.67

ode and an inner (negative) cathode. In the latter, configuration a sizeable fraction[4] of the electrons emitted by the cathode flow axially along the magnetic field lines to ground. The electrons, therefore, do not circulate and do not participate in the rf interaction. Thus, they provide an undesirable "shunt" current[4] which reduces the efficiency of the device. In low voltage magnetrons the shunt current can be suppressed by placing electrostatic shields at both ends of the cathode. However, in high voltage relativistic magnetrons this technique cannot be used because at the large field strengths that exist there ($\gtrsim 200$ kV/cm), all materials emit and arcing occurs readily. The inverted magnetron obviates the problem of the shunt current. With the grounded cathode now on the outside, any electrons flowing axially from the cathode return to it with no loss of energy.

However, in the inverted magnetron configuration, the extraction of the rf power poses a problem. The rf fields are strongest in the vane resonators which are on the inside of the tube and at high electrical potential. One technique[4,12] is to connect the vane resonators by means of slot couplers to a central, coaxial cavity, and transmit the microwave power axially, out the front of the device. This requires a complicated, highly overmoded rf circuit, numerous closely spaced vane resonators and a high voltage isolation transformer.[12] We have chosen a more primitive system in which the rf fields are coupled directly out of the cathode–anode gap and across the electron space charge cloud. This is done by attaching a section of *C* band waveguide to a slot cut in the cathode wall, as is illustrated in Fig. 1. The waveguide is butt mounted with its broad wall aligned along the axis of the magnetron. This orientation couples the axial component of the rf magnetic field in the cathode–anode gap to the rf magnetic field of the TE_{01} mode of the waveguide. The second waveguide shown in Fig. 1 is connected to a matched dummy high-power load; its purpose is to provide a measure of symmetry in the coupling and reduce the possibility of unevenly loading the internal rf structure of the magnetron. The graphite coating on the cathode reduces formation of hot spots and ensures a more uniform electron emission from the surface. As a result, the shot-to-shot reproducibility of the electromagnetic radiation from the magnetron is greatly improved.

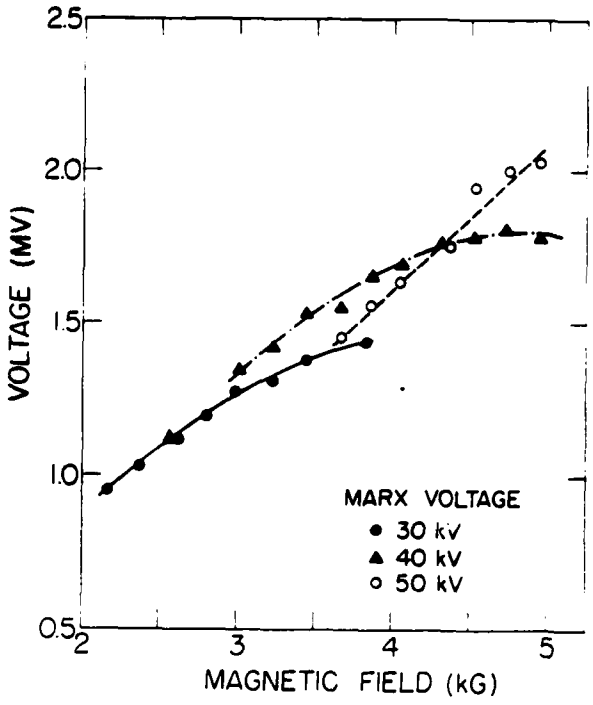

FIG. 2. Voltage as a function of the axial magnetic field for the M8 magnetron.

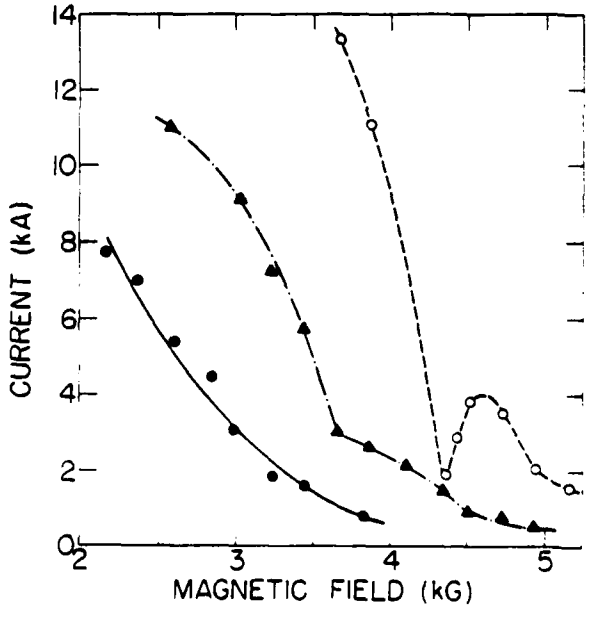

FIG. 3. Current as a function of axial magnetic field for the M8 magnetron (● 30 kV Marx-bank charging; ▲ 40 kV; ○ 50 kV).

II. EXPERIMENT

The electric field between cathode and anode is provided by the Physics International Pulserad 110A high voltage facility. The axial magnetic field is generated[4,10] by two pulsed magnetic field coils surrounding, and coaxial with, the cylindrical electrodes. Typical voltage and current characteristics of the M8 magnetron as function of the axial magnetic field are shown in Figs. 2 and 3, respectively. The three sets of data in each figure correspond to three different Marx generator charging voltages (30, 40, and 50 kV) employed in all of our experiments. The overall voltage–current characteristics are similar to those observed in conventional[3,4] relativistic magnetrons.

The radiation emanating from the magnetron via the *C*-band waveguide is attenuated by ~ 100 dB with the aid of precision calibrated attenuators and directional couplers and is rectified in a calibrated crystal detector. Figure 4 shows the total power emitted as a function of axial magnetic field. We see that power levels in excess of 400 MW are achieved. The bell-shaped curves shown in Fig. 4 are very similar to those obtained for relativistic magnetrons operating in the conventional (noninverted) configuration.[3,4]

The frequency spectrum is measured by means of a solid-state dispersive line[4] having a resolution better than ~ 50 MHz. The observations are plotted in Fig. 5 as a function of the axial magnetic field. It is seen that at low magnetic fields the frequency increases linearly with magnetic field suggesting that one is observing some form of collective cyclotron

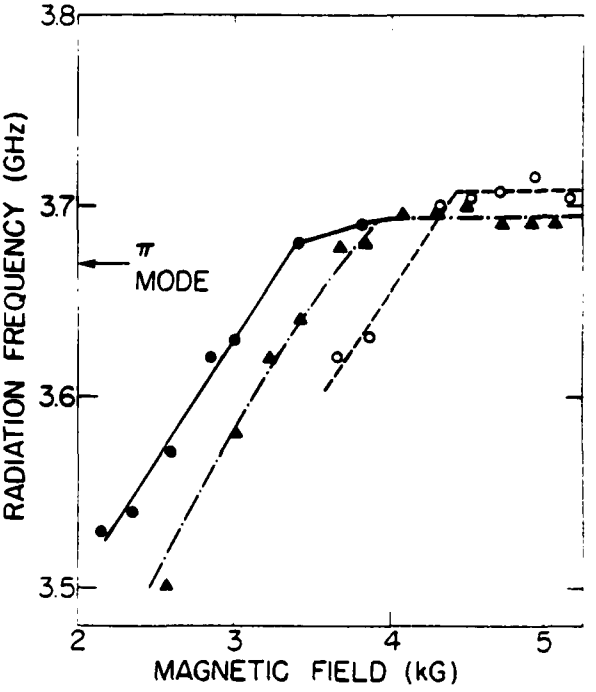

FIG. 5. Radiation frequency as a function of the axial magnetic field for the M8 magnetron (● 30 kV Marx-bank charging; ▲ 40 kV; ○ 50 kV).

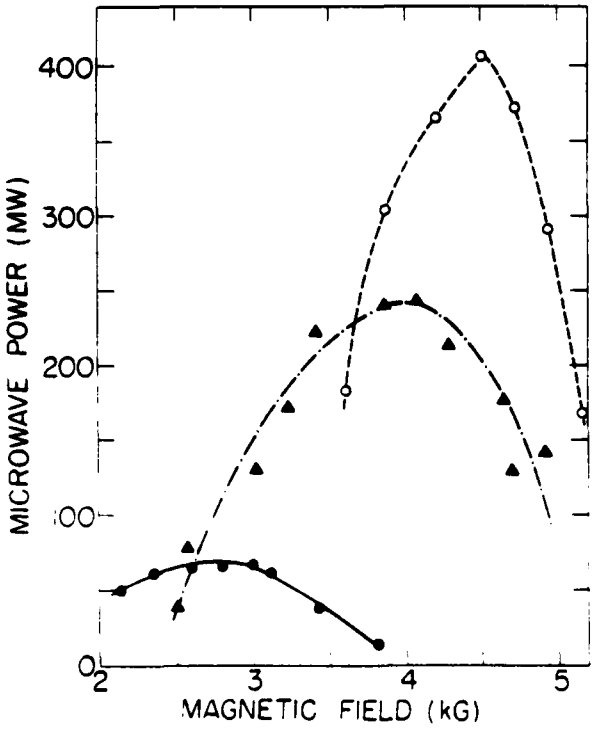

FIG. 4. Radiated power in the 3.2–5.9 GHz frequency range as a function of the axial magnetic field for the M8 magnetron (● 30 kV Marx-bank charging; ▲ 40 kV; ○ 50 kV).

radiation.[13] In this regime of magnetic fields B_z and voltages V (see Fig. 2), B_z is at or a little below the critical magnetic field B_{oc} given by Eq. (1). At higher magnetic fields well above the critical magnetic field B_{oc}, the oscillation frequency becomes virtually independent of B_z as expected when true magnetron oscillations set in. The measured frequency is now close to but slightly higher than the π mode frequency determined by computations and magnetron cold tests (see Table II). The small upward frequency shift relative to the cold test frequency is probably due to the presence of electron space charge in the cathode–anode gap which tends to make the effective gap width smaller and the mode frequency higher. (This is equivalent to "current-pushing" in conventional, nonrelativistic magnetrons.)

Knowledge of the emitted microwave power P_μ, magnetron voltage V, and current I, allow one to derive the tube efficiency defined as the ratio of P_μ / VI. This quantity is plotted in Fig. 6 as a function of the axial magnetic field. The maximum efficiency obtained is $\sim 12\%$.

All observations presented hitherto refer to the eight-vane (M8) magnetron. A similar study of the ten-vane (M10) magnetron reveals characteristics very similar to the M8 device. For example, in the M10, the maximum rf power achieved is 515 MW at an axial magnetic field of 6.65 kG, voltage 1.62 MV, and a current of 9 kA. The resulting efficiency is 3.5%. This is considerably lower than that obtained with the M8 magnetron. Indeed, this lowered efficiency is

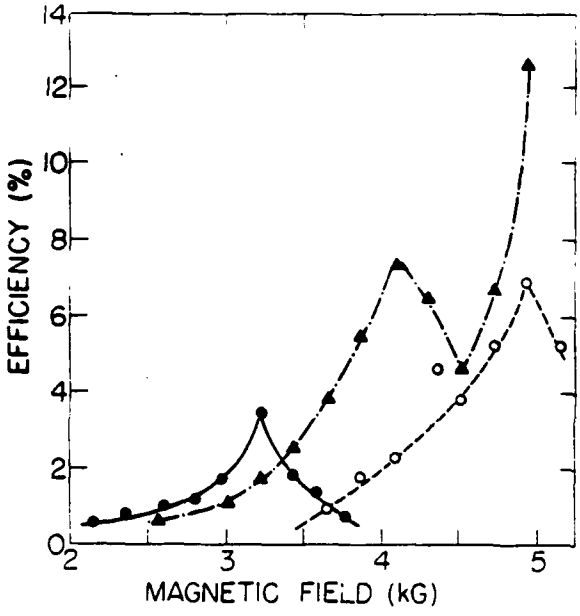

FIG. 6. Magnetron efficiency as a function of the axial magnetic field for the M8 magnetron (● 30 kV Marx-bank charging; ▲ 40 kV; ○ 50 kV).

the main difference between the M10 and M8 devices: although the absolute rf power level obtained from the M10 is equal to or greater than that obtained from the M8 magnetron, the enhanced currents drawn by the former cause an efficiency reduction by a factor of 2 or more.

III. DISCUSSION

We have observed intense ($\sim$400–500 MW) narrow band ($\lesssim$ 50 MHz) microwave radiation at a frequency $\sim$3.7 GHz from an inverted relativistic magnetron which is free from the undesirable shunt currents[4] that often plague magnetrons built in the conventional manner. The available radiation is probably much in excess of what emanates from our simple waveguide-coupled system. Our coupling schema suffers from two defects. First, we couple to the relatively weak radiation field which exists in the cathode–anode gap rather than coupling to fields in the vane resonators. Secondly, a dense electron space-charge cloud intervenes between the output waveguide and the center of the magnetron causing attenuation of the electromagnetic field at the extraction point.

Indeed, we believe that the rf power within the magnetron itself is comparable in magnitude to the power in the electrons. We base this on the results of Fig. 3 where a sharp current increase is seen to occur at a magnetic field ($\sim$4.5 kG) at which the emitted rf power is maximum (Fig. 4). This resonance behavior in the current can occur only if the rf electric field builds up to a level comparable to the externally applied electric field. We note that such current enhancement during strong rf oscillations is typical of the highly efficient, low voltage magnetrons, but has not been seen previously in relativistic magnetrons of the conventional[3–9] (noninverted) type. The fact that this was not seen in previous relativistic magnetrons suggests that rf generation was less efficient, possibly due in part to large axial shunt currents.

A comparison between the large gap (1.38 cm) M8 magnetron and the narrow gap (0.84 cm) M10 magnetron exhibits very similar characteristics, except that the M10 draws more current and its efficiency is smaller by approximately a factor of 2. The lessened efficiency is thought to be due to the fact that a narrow gap partially shorts out the azimuthal component of the rf electric field in the cathode-anode space. Therefore, the device is less conducive[4] to strong space-charge spoke formation (i.e., electron bunching), which is necessary for efficient microwave generation.

ACKNOWLEDGMENTS

This work was supported in part by the Air Force Office of Scientific Research, in part by the Department of the Air Force Aeronautical Systems Division, (AFSC), and in part by the National Science Foundation.

[1] G. B. Collins, ed., *Microwave Magnetrons* (McGraw-Hill, New York, 1948).
[2] E. Okress, ed., *Crossed-Field Microwave Devices* (Academic, New York, 1961), Vols. I and II.
[3] G. Bekefi and T. J. Orzechowski, Phys. Rev. Lett. 37, 379 (1976).
[4] A. Palevsky and G. Bekefi, Phys. Fluids 22, 986 (1979).
[5] A. Palevsky, G. Bekefi, and A. T. Drobot, J. Appl. Phys. 52, 4938 (1981).
[6] N. F. Kovalev, B. D. Kol'chugin, V. E. Nechaev, M. M. Ofitserov, E. I. Soluyanov, and M. I. Fuks, Pis'ma Zh. Tekh. Fiz. 3, 1048 (1977) [Sov. Tech. Phys. Lett. 3, 430 (1977)]; V. E. Nechaev, M. I. Petelin, and M. I. Fuks, Pis'ma Zh. Tekh. Fiz.3, 763 (1977) [Sov. Tech. Phys. Lett. 3, 310 (1977)].
[7] A. N. Didenko, A. S. Sulakshin, G. P. Fomenko, Yu. G. Shtein, and Yu. G. Yushkov, Pis'ma Zh. Tekh. Fiz. 4, 10 (1978) [Sov. Tech. Phys. Lett. 4, 3 (1978)].
[8] G. Craig, J. Pettibone, and D. Ensley, Proceedings IEEE International Conference on Plasma Science (IEEE Cat. No. 79Ch 1410-ONPS) (1979), p. 44.
[9] I. Z. Gleizer, A. N. Didenko, A. S. Sulakshin, G. P. Fomenko, and V. I. Tsvetkov, Pis'ma Zh. Tech. Fiz. 6, 44 (1980) [Sov. Tech. Phys. Lett. 6, 19 (1980)].
[10] T. J. Orzechowski and G. Bekefi, Phys. Fluids 19, 43 (1976); 22, 978 (1979).
[11] J. F. Hull, *Crossed-Field Microwave Devices*, edited by E. Okress (Academic, New York, 1961), Vol. II, p. 291.
[12] R. K. Parker, W. M. Black, R. A. Tobin, and G. Farney, Proceedings of

the IEEE International Conference on Plasma Science (IEEE Cat. No. 79CH1410-ONPS), 1979), p. 44; IEDM. Tech. Digest, 175 (1979).

[13]We note that at or near Brillouin equilibrium the ratio of the cyclotron to plasma frequencies is constant and approximately equal to unity. Thus, the observed radiation at low B_z may well be connected with collective plasma oscillations.

END

FILMED

3-84

DTIC